Passive dynamics explain quadrupedal walking, trotting, and tölting

Gan, Zhenyu ; Wiestner, Thomas ; Weishaupt, Michael A ; Waldern, Nina M ; David Remy, C

Abstract: This paper presents a simplistic passive dynamic model that is able to create realistic quadrupedal walking, tölting, and trotting motions. The model is inspired by the bipedal spring loaded inverted pendulum (SLIP) model and consists of a distributed mass on four massless legs. Each of the legs is either in ground contact, retracted for swing, or is ready for touch down with a predefined angle of attack. Different gaits, that is, periodic motions differing in interlimb coordination patterns, are generated by choosing different initial model states. Contact patterns and ground reaction forces (GRFs) evolve solely from these initial conditions. By identifying appropriate system parameters in an optimization framework, the model is able to closely match experimentally recorded vertical GRFs of walking and trotting of Warmblood horses, and of tölting of Icelandic horses. In a detailed study, we investigated the sensitivity of the obtained solutions with respect to all states and parameters and quantified the improvement in fitting GRF by including an additional head and neck segment. Our work suggests that quadrupedal gaits are merely different dynamic modes of the same structural system and that we can interpret different gaits as different nonlinear elastic oscillations that propel an animal forward.

DOI: https://doi.org/10.1115/1.4030622

Journal of Computational and Nonlinear Dynamics. Received February 10, 2015;
Accepted manuscript posted May 14, 2015. doi:10.1115/1.4030622

Passive Dynamics Explain Quadrupedal Walking, Trotting, and Tölting

Zhenyu Gan
Robotics and Motion Laboratory
Department of Mechanical Engineering
University of Michigan
Ann Arbor, Michigan, 48109
Email: ganzheny@umich.edu

Thomas Wiestner
Michael A. Weishaupt
Nina M. Waldern
Equine Department
Vetsuisse Faculty
University of Zurich
Zurich, CH-8057
Switzerland
Email: twiestner@vetclinics.uzh.ch
Email: mweishaupt@vetclinics.uzh.ch
Email: nwaldern@vetclinics.uzh.ch

C. David Remy
Robotics and Motion Laboratory
Department of Mechanical Engineering
University of Michigan
Ann Arbor, Michigan, 48109
Email: cdremy@umich.edu

This paper presents a simplistic passive dynamic model that is able to create realistic quadrupedal walking, tölting, and trotting motions. The model is inspired by the bipedal SLIP model and consists of a distributed mass on four massless legs. Each of the legs is either in ground contact, retracted for swing, or is ready for touch down with a predefined angle of attack. Different gaits, that is, periodic motions differing in interlimb coordination patterns, are generated by choosing different initial model states. Contact patterns and ground reaction forces (GRFs) evolve solely from these initial conditions. By identifying appropriate system parameters in an optimization framework, the model is able to closely match experimentally recorded vertical GRFs of walking and trotting of Warmblood horses, and of tölting of Icelandic horses. In a detailed study, we investigated the sensitivity of the obtained solutions with respect to all states and parameters, and quantified the improvement in fitting ground reaction force by including an additional head and neck segment. Our work suggests that quadrupedal gaits are merely different dynamic modes of the same structural system and that we can interpret different gaits as different nonlinear elastic oscillations that propel an animal forward.

Nomenclature

m_o Total mass
l_o Uncompressed leg length
g Gravitational constant
l_1 Main body length
j_1 Main body inertia
k_F Forelimb spring stiffness
k_H Hind limb spring stiffness
α_F fore angle of attack
α_H Hind angle of attack
d_{COM} Offset of the COM of the main body
t_{swing} swing time
m_1 Main body mass
m_2 Head mass
l_2 Head length
j_2 Head inertia
k_{head} Head-neck spring stiffness
θ_{rest} Head resting angle

1 Introduction

Modeling, simulating, and understanding the dynamics of locomotion in all its detail requires multi-body models with a large number of degrees of freedom, the correct handling of intermitted ground contact with collisions, and the modeling of a substantial amount of soft-body motion. These models have to incorporate neural control and they must account for the highly non-linear characteristics of muscle actuation. For most purposes, such a detailed representation is not necessary. On the contrary, while complex models could

precisely represent all the details of locomotion in nature, they would have difficulties to reveal the underlying principles. Because of this, locomotion research often relies on *simplistic passive models* [1, 2, 3]. These models are highly abstract approximations of reality, often reducing the entire system to a single point mass. Still, they are able to capture the essential dynamics of locomotion. In the past, such simplistic models have successfully been used in the analysis of energetic efficiency [4,5], or in the quantification of dynamic stability [6, 7].

In recent research, a *unified* model was proposed to explain the underlying dynamics of bipedal walking and running [8]. It is based on the Spring Loaded Inverted Pendulum (SLIP) model [9, 10]. This spring mass model assumes that a point mass is connected via a massless linear spring with stiffness k to an equally massless foot. During stance, the mass pivots about the contact point while the spring is undergoing cyclic compression and extension. Since the leg has no mass, no swing dynamics exist, and it is assumed that the leg simply moves to a predefined angle of attack α during swing. A model similar to the SLIP model, but with *two* legs, can explain the GRFs of both human walking and running; and it can do so with a single set of parameters. In this model, the point mass is mounted on two independent, massless springs of equal rest length, angle of attack, and stiffness. As opposed to stiff legged systems, which require an instantaneous transfer of support, the two legs can conduct touch down and lift off independently, such that a double stance phase as well as an airborne phase are possible. The GRFs that are predicted by this model closely resemble those of human walking and running [11], and the model is able to explain the characteristic double hump in the vertical GRFs of human walking [12].

This paper extends this work to quadrupedal locomotion, and is specifically aiming at the large variety of gaits that are used by quadrupeds. It builds on our previous work, in which we have studied passive dynamic walking with stiff legs [13]. We identified two-beat and four-beat walking gaits, and investigated their dynamics and stability in two- and three-dimensional models [14, 15]. The main body and the legs in these models were represented by rigid links. Since motion was based on inverted pendulum walking, the range of possible gaits was severely limited. Stiff legged systems require an instantaneous transfer of support, which means that exactly two of the four legs are on the ground at all times. With these models it was hence only possible to identify *symmetrical* gaits with a duty factor of $\beta = 0.5$. Inverted pendulum walking by itself is not able to capture the rich variety of gaits and locomotion patterns that can be found in nature.

This is not surprising, given that the compliance of the locomotor apparatus plays such an important role in quadrupedal locomotion in nature. [16], for example, pointed out that the long flexor tendons of the horse's limbs can store and release elastic energy during the stance phase, similar to a spring. Their experiments showed that during weight-bearing the limb changes its length by flexion of limb joints, particularly the metacarpophalangeal joint, and therefore can be modeled as a compression spring. [17] showed that metacarpophalangeal joint angles changed proportionally with peak vertical GRF.

The current paper is based on this insight, and investigates quadrupedal locomotion with a simplistic model with compliant legs. The legs are connected to the shoulder and hip of a rigid main body, which –in contrast to the original SLIP model– has a distributed mass. To obtain a well-defined sequence of ground contact, we defined three distinct phases for each leg: *stance*, *swing*, and *ready for touch down*. In the *ready for touch down* phase each leg goes to a predefined angle of attack, similar to the SLIP model. This phase is, however, preceded by an extended *swing* phase in which the legs cannot make contact. This variation of the original SLIP model was necessary to enable a coordinated motion of the four legs. In a numerical framework for gait creation [18], we identified periodic motions in a single-shooting implementation. The contact sequence was thereby an outcome of the numerical integration, and was not determined a priory. With this, we produced a wide variety of gaits by simply changing the initial states and system parameters. Furthermore, by numerically fitting the model-predicted GRFs to experimentally obtained data, we were able to automatically identify appropriate values for these states and parameters. These data was obtained on an instrumented high-speed treadmill.

With this approach, we are the first that are able to produce realistic walking, trotting, and tölting with a *single* conceptual model. Furthermore, the model-predicted vertical GRFs closely matched the recorded GRFs of walking and trotting Warmblood horses, and of tölting Icelandic horses. Our results suggest that the different quadrupedal gaits that are found in nature are potentially just different oscillation modes of the same dynamic system. The paper highlights the significance of natural dynamic motions and of elastic energy storage in quadrupedal locomotion.

In the remainder of this paper, we will introduce the mathematical details of the dynamic modeling, gait creation, and fitting to recorded GRFs. We will report on the gaits that we found and quantitatively compare the identified motion and morphological parameters to those of horses. In a sensitivity study, we examine how well different parameters can be identified by our methodology and how much influence they have on a particular gait. As a possible extension to the simplistic model presented above, we evaluate an extended model with an articulated head-neck segment. This model predicts the GRFs of walking more accurately.

2 Methods

In this section, we introduce the theoretical framework and the simplistic models that are used to generate periodic motions that optimally predict experimentally recorded GRFs. The methodology is based on our previous work on optimal gait creation [18, 19].

2.1 Gait Creation

A gait is simply defined by a vector of initial states $\mathbf{X} = [\mathbf{q}_o, \dot{\mathbf{q}}_o, \mathbf{z}_o]^{\mathrm{T}}$, and a vector of system parameters $\mathbf{p}$. $\mathbf{q} = [x, y, \varphi]^{\mathrm{T}}$ is the generalized coordinate vector of the model. It contains the horizontal and vertical position (x, y) of the center of mass (COM), as well as the orientation of the main body φ. The continuous dynamics of the model are governed by the equations of motion (*EOM*):

$$\ddot{\mathbf{q}} = f(\mathbf{q}, \dot{\mathbf{q}}, \mathbf{z}, \mathbf{p}). \tag{1}$$

The vector $\mathbf{z}$ defines the discrete states of the system, which has a derivative of 0. This state only changes when a foot touches down or leaves the ground. We refer to such instances as *events*, which are defined by the directional zero crossing of an event function e:

$$e(\mathbf{q}, \dot{\mathbf{q}}, \mathbf{z}, \mathbf{p}) = 0, \quad \text{with} \quad \dot{e} > 0. \tag{2}$$

One event is defined as the *terminal event* $e^\star$ and marks the end of a stride. The discrete states $\mathbf{z}$ change according to an event-handler function:

$$\mathbf{z}^+ = g\left(\mathbf{q}, \dot{\mathbf{q}}, \mathbf{z}^-, \mathbf{p}\right), \tag{3}$$

where the indices $-$ and $+$ indicate the states right before and right after the event. The discrete state vector $\mathbf{z}$ is given by $\mathbf{z} = [\mathbf{phase}, \mathbf{pos}_x]^{\mathrm{T}}$ and contains two kinds of discrete states: A first set is used to track the *phase* of each leg i ($phase_i \in [1,2,3]$); that is, the states record if the leg is *ready for touch down* (1), in *stance* (2), or in *swing* (3). The second set of discrete states $pos_{x,i}$ is used to record the horizontal positions at which a foot touched the ground. From these positions, we calculate the spring forces that the stance legs exhibit and we monitor whether foot placement is periodic over the course of multiple strides. The continuous states $\mathbf{q}$ and $\dot{\mathbf{q}}$ do normally not change during events. The only exception is the terminal event $e^\star$, in which the horizontal position is reset to $x = 0$, and all horizontal foot positions $pos_{x,i}$ are shifted accordingly. This removes all forward motion from a stride and creates a fully periodic motion.

To simulate a stride, we start with the initial state values $\mathbf{q}_o$, $\dot{\mathbf{q}}_o$ and $\mathbf{z}_o$ at time $t = 0$. State derivatives are computed according to the equations of motion (1) and are being integrated while continuously monitoring for events (2). Each event is processed by the appropriate event handler function (3), before integration is continued with the new values of the discrete states $\mathbf{z}^+$. This process is repeated until the terminal event $e^\star$ is triggered. With this, we define a stride-to-stride mapping $\mathbf{X}^{k+1} = \mathrm{P}\left(\mathbf{X}^k, \mathbf{p}\right)$, which conducts the simulation of a single stride starting from the values $\mathbf{X}^k$ at the beginning of a stride. It returns the values $\mathbf{X}^{k+1}$ at the end of the stride. For a periodic motion, $\mathbf{X}^k$ and $\mathbf{X}^{k+1}$ are equal, which reduces the definition of a periodic gait to solutions of the equation:

$$\mathrm{P}(\mathbf{X}, \mathbf{p}) - \mathbf{X} = 0. \tag{4}$$

During the simulation of a stride, we also compute the simulated GRFs $\mathrm{F}_{sim}(t, \mathbf{X}, \mathbf{p})$. They are a function of time t and depend on the parameters $\mathbf{p}$ and on the states at the beginning of the stride as defined by $\mathbf{X}$. $\hat{\mathrm{F}}(t)$ denotes the experimentally obtained GRFs that were recorded from actual horses. To quantify how well the simplistic model predicts the experimentally obtained GRFs, we define the residual:

$$\mathrm{c}(\mathbf{X}, \mathbf{p}) = \int_0^1 \left\| \mathrm{F}_{sim}(s, \mathbf{X}, \mathbf{p}) - \hat{\mathrm{F}}(\hat{s}) \right\|^2 dt. \tag{5}$$

The integral uses a normalized time $s = \frac{t}{t_{stride}}$ ($\hat{s} = \frac{t}{\hat{t}_{stride}}$) which runs from 0 to 1 for both the simulated and the experimentally recorded stride. This normalization allowed an easier comparison of simulated and experimental data. One should note, that this means that the cost has no notion of *absolute* time. Since the primary goal of this research is the prediction of the correct footfall sequence (i.e., of *relative* time) as well as of the correct shapes of the vertical GRFs, we deemed this an acceptable simplification. The value of the integrated residual is used as a cost function in a constrained optimization problem:

$$\begin{aligned} &\min\{\mathrm{c}(\mathbf{X}, \mathbf{p})\} \\ s.t. \quad &\mathrm{P}(\mathbf{X}, \mathbf{p}) - \mathbf{X} = 0 \end{aligned} \tag{6}$$

that finds states and parameters that optimally predict experimentally recorded GRFs. The optimization problem is solved numerically with the MATLAB optimization toolbox using a Sequential Quadratic Programming (SQP) algorithm [18].

2.2 Models

The simplistic model consists of a rigid main body and four massless elastic legs (Fig. 1a). It is planar with all motion being restricted to the sagittal plane.

The main body measures l_1 from hip to shoulder. It has a mass of m_o and an inertia of j_1. The COM can be displaced along the anteroposterior axis to represent different weight distributions. A parameter $d_{COM} (0 < d_{COM} < 1)$ is used to continuously shift the COM from the shoulder ($d_{COM} = 1$) to the hip ($d_{COM} = 0$). The distances from the COM to the shoulder and hip are given by:

$$d_F = l_1 \cdot (1 - d_{COM}); \quad d_H = -l_1 \cdot d_{COM}. \tag{7}$$

With this, the shoulder (hip) positions of each leg i are calculated as:

$$\begin{aligned} x_i &= x + d_i \cdot cos(\varphi) \\ y_i &= y + d_i \cdot sin(\varphi), \end{aligned} \tag{8}$$

where $d_i = d_F$ for the forelimbs and $d_i = d_H$ for the hind limbs (Note: d_H is negative). The legs are modeled as massless springs (forelimb stiffness k_F, hind limb stiffness k_H,

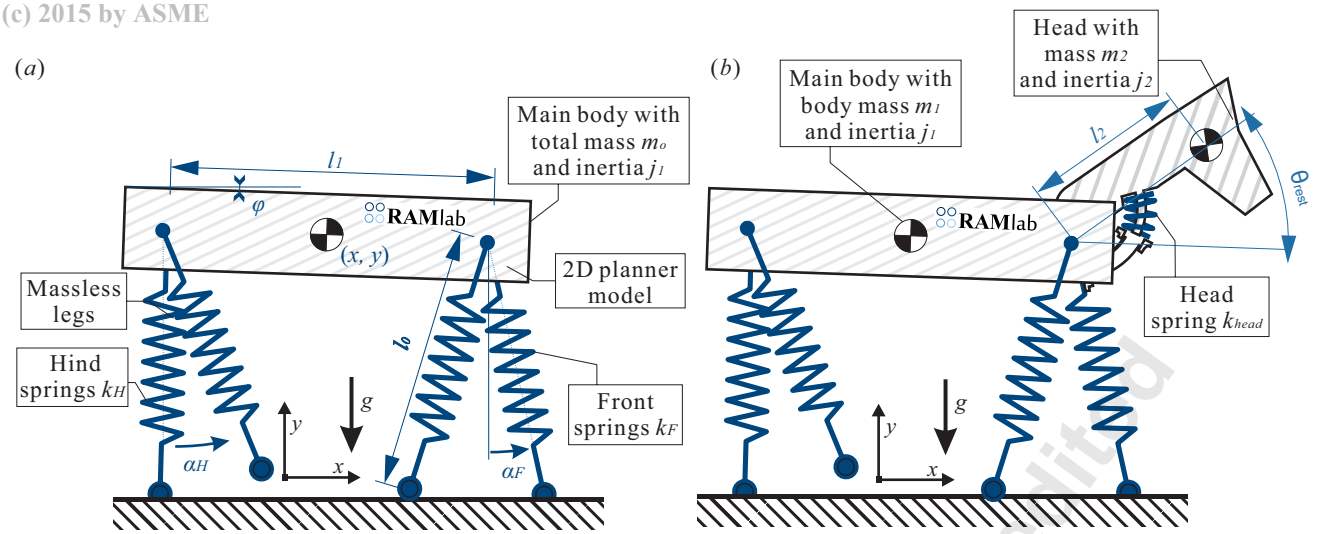

Fig. 1. A simplistic model that essentially consists of a single distributed mass on four mass-less springs is able to explain the dynamics of quadrupedal walking, trotting, and tölting (shown in a). In addition, we studied an extended version that includes a head-neck segment connected to the body by a rotational joint with a torsional spring (shown in b).

no damping) with an uncompressed length of l_o. They are connected to the main body at the hip and shoulder via rotational joints. Since the legs have no mass, it is assumed that they go to a pre-defined *angle of attack* during swing. This angle is given by α_F for the forelimbs and by α_H for the hind limbs. Furthermore, there are no collision losses and the model is energetically conservative. Feet are modeled as points and we assume that the feet never slip on the ground. The system parameters $\mathbf{p}$ include the main body length l_1, the main body inertia j_1, the forelimb and hind limb spring stiffness (k_F, k_H), the offset of the COM of the main body/torso d_{COM} and the angle of attack (α_F for forelimbs and α_H for hind limbs). Finally, $\mathbf{p}$ includes a swing time t_{swing}, during which a leg is not able to engage in ground contact.

$$\mathbf{p} = [l_1,\, j_1,\, k_F,\, k_H,\, d_{COM},\, \alpha_F,\, \alpha_H,\, t_{swing}]^T. \tag{9}$$

Parameter values are given in units normalized relative to total mass m_o, uncompressed leg length l_o and gravity g. As these three quantities are removed from the set of adjustable parameters, results become more general [20].

Head and neck motion play an important role in quadrupedal locomotion. To make sure our model is not oversimplified, we additionally studied a headed model (Fig. 1b) in which we use a second rigid body to represent head and neck. This body is connected to the shoulder via a rotational joint with a torsional spring. Head and neck have a mass of m_2 and an inertia of j_2. The stiffness of the head-neck spring is k_{head}. During locomotion, head and neck passively rotate about the shoulder joint. There is no damping associated with this joint. The resting angle is θ_{rest} and the spring creates a torque of $M_{head} = k_{head}(\theta_{rest} - \theta)$. The extended parameter vector $\mathbf{p}$ is given by:

$$\mathbf{p} = [l_1,\, j_1,\, k_F,\, k_H,\, d_{COM},\, \alpha_F,\, \alpha_H,\, t_{swing},\, m_2,\, l_2,\, j_2,\, k_{head},\, \theta_{rest}]^T. \tag{10}$$

Since all masses are normalized to total body mass m_o, the main body mass is given by $m_1 = m_o - m_2$ and is thus not part of the free parameter vector.

2.3 System Dynamics

The equations of motion are stated in the canonical form

$$\mathbf{M}(q)\ddot{q} + \mathbf{h}(q,\, \dot{q}) = \tau, \tag{11}$$

where $\mathbf{M}(q)$ is the mass matrix, $\mathbf{h}(q,\dot{q})$ are the Coriolis, centrifugal, and gravitational terms, and τ is the vector of generalized forces. The latter is created by the spring forces of all legs i that are in stance. These forces act along the direction of the leg γ_i with a magnitude F_i that is proportional to the leg compression $l_o - l_i$. The stiffness of this spring is given by k_i:

$$\begin{aligned} l_i &= \sqrt{(x_i - pos_{x,i})^2 + y_i^2} \\ F_i &= k_i \cdot (l_o - l_i) \\ \gamma_i &= arctan\left(\frac{pos_{x,i} - x_i}{y_i}\right) \end{aligned} \tag{12}$$

The vector of generalized forces τ is computed as a projection of the spring forces $\tau = \sum_i \mathbf{J_i}^T F_i$ with

$$\mathbf{J}_i = [-\sin(\gamma_i),\, \cos(\gamma_i),\, d_i \cdot cos(\varphi - \gamma_i)] \tag{13}$$

Table 1. List of model parameters. All values are normalized with respect to total mass m_o, uncompressed leg length l_o, and the gravitational constant g

Param.	Unit	Description
m_o	$[\cdot]$	Total mass
l_o	$[\cdot]$	Uncompressed leg length
g	$[\cdot]$	Gravitational constant
l_1	$[\mathrm{l_o}]$	Main body length
j_1	$[\mathrm{m_o l_o^2}]$	Main body inertia
k_F	$[\mathrm{m_o g / l_o}]$	Forelimb spring stiffness
k_H	$[\mathrm{m_o g / l_o}]$	Hind limb spring stiffness
α_F	[rad]	fore angle of attack
α_H	[rad]	Hind angle of attack
d_{COM}	$[\mathrm{l_o}]$	Offset of the COM of the main body
t_{swing}	$[\sqrt{\mathrm{l_o/g}}]$	swing time
m_1	$[\mathrm{m_o}]$	Main body mass
m_2	$[\mathrm{m_o}]$	Head mass
l_2	$[\mathrm{l_o}]$	Head length
j_2	$[\mathrm{m_o l_o^2}]$	Head inertia
k_{head}	$[\mathrm{m_o g l_o / rad}]$	Head-neck spring stiffness
θ_{rest}	[rad]	Head resting angle

for the headless model. As this model is a single body system, the mass matrix is simply a diagonal matrix with entries $\mathbf{M} = diag(m_1,\ m_1,\ j_1)$, and $\mathbf{h}$ only contains the gravitational forces: $\mathbf{h} = [0,\ -m_o g,\ 0]^T$. The equations of motion for the headed model are a bit more involved. They were derived using Euler-Lagrange equations, and the components $\mathbf{M}$, $\mathbf{h}$, and $\mathbf{J}_i$ are reported in Appendix A.

Each leg is in one of three discrete phases $phase_i$: *ready for touch town* (1), *stance* (2), or *swing* (3), and the transition between these phases is detected via the following event detection functions:

$$\begin{aligned} e_{i,1} &= l_o \cdot cos(\alpha_i) - y_i \\ e_{i,2} &= l_i - l_o \\ e_{i,3} &= t_i - t_{swing} \end{aligned} \tag{14}$$

In the corresponding event handler functions, the phase of the involved leg is updated to its new value. At touchdown, the contact position pos_x is updated according to $g_{i,1}$, and at liftoff, the time measurement of the swing phase is reset.

$$\begin{aligned} g_{i,1} &: phase_i^+ = 2,\ pos_{x,i}^+ = x_i + l_i \cdot sin(\alpha_i) \\ g_{i,2} &: phase_i^+ = 3,\ t_i^+ = 0 \\ g_{i,3} &: phase_i^+ = 1 \end{aligned} \tag{15}$$

2.4 Experimental Data

The experimental data were recorded on an equine high-speed treadmill (Mustang 2200, Kagra AG) instrumented with piezoelectric force transducers (Type Z17135, Kistler Instruments) and able to measure vertical GRF of all four limbs simultaneously [21]. Recordings were made with a clinically sound and treadmill-adapted Warmblood riding horse (withers height: 1.74 m, m_o: 660 kg) at walk (1.7 m/s) and trot (3.4 m/s) and an Icelandic horse (withers height: 1.35 m, 355 kg) at the tölt (3.3 m/s). Both horses showed representative breed-specific movement patterns. The active leg length was set to be $l_o = 0.135 \times m_o^{0.37}$, which equaled to about 85 % of the horses' withers height [22]. In contrast to real horses, the model has the same leg length for all four limbs. Data collection lasted 20 seconds at a sampling frequency of 480 Hz. Force-time histories were analyzed with in-house developed software (HP2, Equine Performance Centre, University of Zurich) which allowed automatic extraction of force, time and spatial parameters for each limb separately. Twenty succeeding motion cycles per horse were analyzed and averaged. Force parameters were normalized to the horse's bodyweight.

2.5 Sensitivity Analysis

To be able to judge how well each parameter could be identified by our optimization approach, we conducted a detailed sensitivity study for each gait. Looking at a single initial condition X_j (or a single parameter p_j) at a time, we varied its value by some δX (δp) and then fixed it while optimizing all other states and parameters. Assuming that $\mathbf{x}^\star$ and $\mathbf{p}^\star$ are solutions to the optimization problem (6) (with a final cost value of $c^\star$), this is equivalent to stating a new optimization problem with an additional constraint:

$$\begin{aligned} & \min \{\mathrm{c}(\mathbf{X}, \mathbf{p})\} \\ s.t. \quad & \mathrm{P}(\mathbf{X}, \mathbf{p}) - \mathbf{X} = 0 \\ & X_j = X_j^\star + \delta X_j \end{aligned} \tag{16}$$

The cost value c at the solution of this optimization problem is a direct function of δX_j. The increase in cost from $c^\star$ to $c(\delta X_j)$, indicates how sensitive the process is with regard to X_j; or -in other words- how well a particular state can be identified. If the variation of a certain state does create a large increase in cost, it means that the state can be identified clearly in the original optimization. If, on the other hand, a certain state does not create an increase in cost, it can be changed without reducing the quality of the fit. Such a state cannot be identified by our proposed method. We can draw similar conclusions about parameters p_j.

Table 2. Coefficients of determination (R^2) of the model-predicted GRFs. Values are listed for both, the model without a head and that with an articulated head and neck

Gaits	left hind	right hind	left fore	right fore
Headless Walk	0.922	0.897	0.958	0.957
Headless Tölt	0.979	0.986	0.998	0.967
Headless Trot	0.999	0.998	0.999	0.999
Headed Walk	0.978	0.971	0.982	0.977
Headed Tölt	0.967	0.962	0.992	0.989
Headed Trot	0.999	0.998	0.999	0.999

3 Results

We applied the methods and models described in Section 2 to synthesize three different gaits: Walk and trot of Warmblood horses, as well as tölt of Icelandic horses. We were able to produce all three gaits with the same conceptual model, while accurately predicting the experimentally recorded contact timing and GRFs (Table 2). Mathematically, the three gaits are defined by their initial continuous and discrete states (as given by $\mathbf{X}$, Table 3 & 4) as well as their system parameters (given by $\mathbf{p}$, Table 5 & 6). The complete motion evolves fully from these values.

In this section, we highlight some key-features of our algorithm, report on the properties of the three identified gaits, and discuss the sensitivity of the solutions with respect to individual model parameters and initial states. Furthermore, we analyze the results obtained by a model with an articulated head-neck segment, and quantify how important this additional model component is in the prediction of the ground contact forces.

3.1 Identified Motions and Parameters

For the optimization problem of eq. (6) to converge, one must find a suitable initial guess for $\mathbf{X}$. This initial guess must show a footfall sequence that is similar to the experimentally recorded data and must result in a motion that is fairly close to being periodic. Particularly problematic are *missed* or *redundant* events; that is, feet that either do not touch the ground at all or that make contact more than once. The timing of the swing phase (defined by t_{swing}) was tuned towards avoiding these situations. Missed or redundant events otherwise cause discontinuities in the root function $\mathrm{P}(\mathbf{X},\mathbf{p})-\mathbf{X}=0$, which makes it impossible for the SQP solver to converge. Since we were relying on a single shooting method for optimization, the regions of possible initial model states are quite narrow. It thus took some directed trial and error to find appropriate initial guesses for the model states.

Once a suitable initial guess has been determined, the optimization converged in less than 1 minute on a standard Desktop PC. One should note that the optimization problem of eq. (6) is non-convex. There is no guarantee that the SQP solution represents a global minimum. To avoid local minima as much as possible, we conducted optimizations starting from multiple initial guesses. In combination with the sensitivity study of Section 2.5, this gave us some confidence that our solutions are globally optimal. As an example of the periodic continuous state trajectories that result from this process, the motion of the main body and the head-neck segment are shown over a full stride of walking, tölting, and trotting in Figure 2.

The most characteristic property of a gait, the footfall sequence is given by the discrete **phase** states (Fig. 3). The transition from *ready for touch down* ($phase_i = 1$) to *stance* ($phase_i = 2$) is detected kinematically. A *touch-down* event happens if the contact foot height goes to zero. During this event, the horizontal position of the contact point ($pos_{x,i}$, shown by the solid line) is updated to reflect the new contact point. *Lift-off* is also detected kinematically. A leg leaves the ground, if it would be extending beyond its rest length l_o. At this moment the timer that measures swing time (illustrated by the red dotted lines) is reset to zero and a *swing* phase of duration t_{swing} is initiated ($phase_i = 3$). A timer triggers the *swing over* event when its value equals to t_{swing}. From a dynamic point of view, there is no distinction between *swing* and the *ready for touch down* phase. In both cases, the legs are assumed to be in the air and are not creating any forces on the main body. The difference is that during the *swing* phase the leg is not able to engage in ground contact. This prevents feet from striking the ground prematurely and enables a coordinated motion of the four legs.

In our framework, the end of a stride is marked by the *lift-off* of the right forelimb (the *terminal event* $e^\star$). Since legged motion is periodic, one should note that any event or relative time point in the cyclic movement might serve as a stride boundary. Our particular choice implies that the right forelimb must always be started in *swing*, right after lift-off. The initial phases of the other legs can be defined freely, and each different combination results in a different footfall pattern. To achieve quadrupedal *walking*, for example, we have to start the two left limbs in *stance* and the right hind limb in *swing* (Table 4).

To better visualize the result, a sequence of animated frames of the walking gait is shown in Figure 4 [1]. For purposes of visualization, the swing legs are shown as being retracted and moving gradually towards the angle of attack; despite the fact that in the mathematical model swing happens instantaneously. Once the limbs are ready for touch down, they are shown as being uncompressed and at the angle of attack. Finally, a leg that is in stance is indicated by a filled circle at the foot. At this time, the spring is engaged and creates force.

[1] Videos of all gaits are available in the supporting online documents

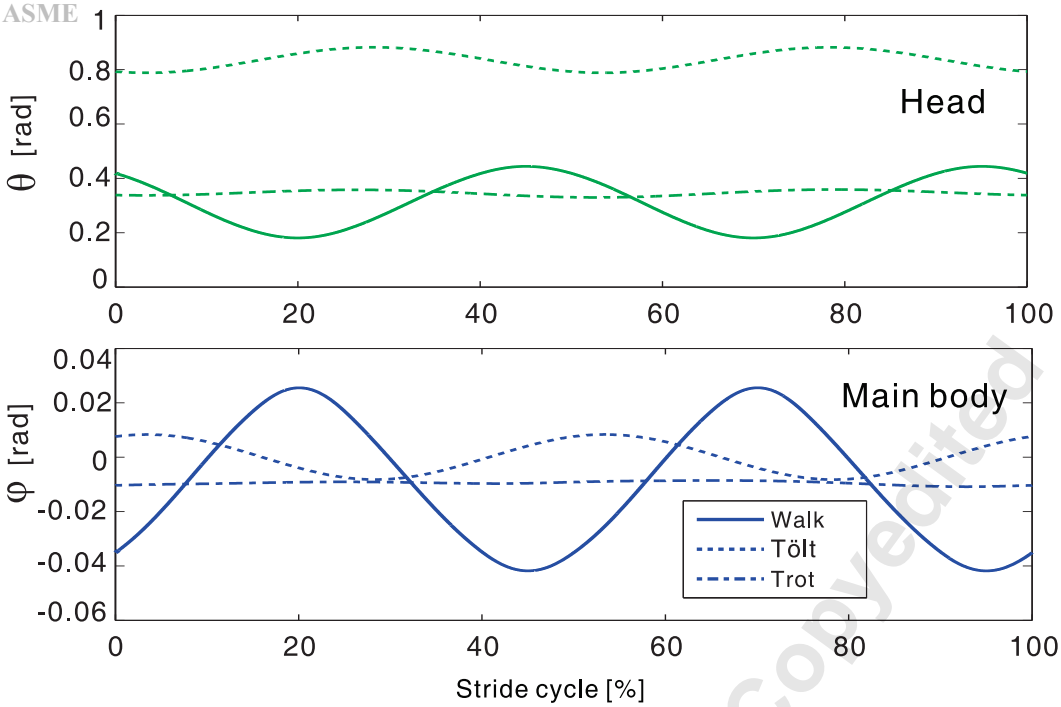

Fig. 2. Head-neck angle (top), and main body angle (bottom) of a single stride at walk, tölt, and trot for the headed model. Oscillation amplitudes change with gait and are most pronounced in the walk. Generally, the head and torso angles are 180° out of phase. That is, the head is low if the shoulders are high. A similar behavior is observed in horses.

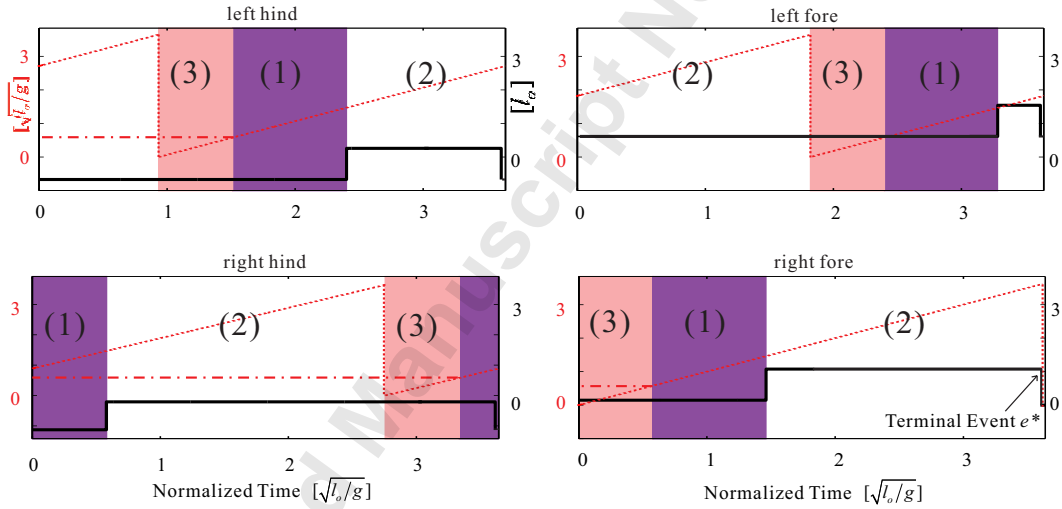

Fig. 3. The discrete states of all four limbs are shown for a single stride of walking of the headless model. The different phases of each leg are *ready for touch down* (1), *stance* (2), and *swing* (3). At the beginning of *swing*, a timer is started (dotted red line) that triggers the transition into *ready for touch down* once it reaches t_{swing}. All four limbs share the same t_{swing} value that is illustrated by red dash-dotted line. The associated waiting period prevents feet from striking the ground too early and allows for a coordinated motion of the model's legs. The absolute horizontal position of the foot on the ground (solid black line) is only updated at touchdown and remains constant throughout the other phases. At the terminal event, the forward motion is removed from this variable, making it periodic from step to step.

3.1.1 Walk

The walk is a symmetrical four-beat gait with the footfall sequence: right hind, right fore, left hind, left fore. Phases of bipedal support alternate with tripedal support phases, and the vertical GRFs show the characteristic double hump that results from a midstance relieve (Fig. 5a, b). During walking, the leg springs undergo two compression-extension cycles that create this force profile. The mechanism is similar to what can be observed in the bipedal SLIP model [23]. The double-compression of each leg is accompanied by a pronounced pitching motion (-1.45° $+1.23^\circ$) of the main body (φ in Fig. 2). The walk had a velocity of 0.255 $\sqrt{l_{og}}$ in simulation, compared to 0.457 $\sqrt{l_{og}}$ in the experimental data.

The model accurately predicts the sequence and timing of the contact events. Furthermore, the model-predicted GRFs for each individual foot roughly match the experimen-

Journal of Computational and Nonlinear Dynamics. Received February 10, 2015;
Accepted manuscript posted May 14, 2015. doi:10.1115/1.4030622

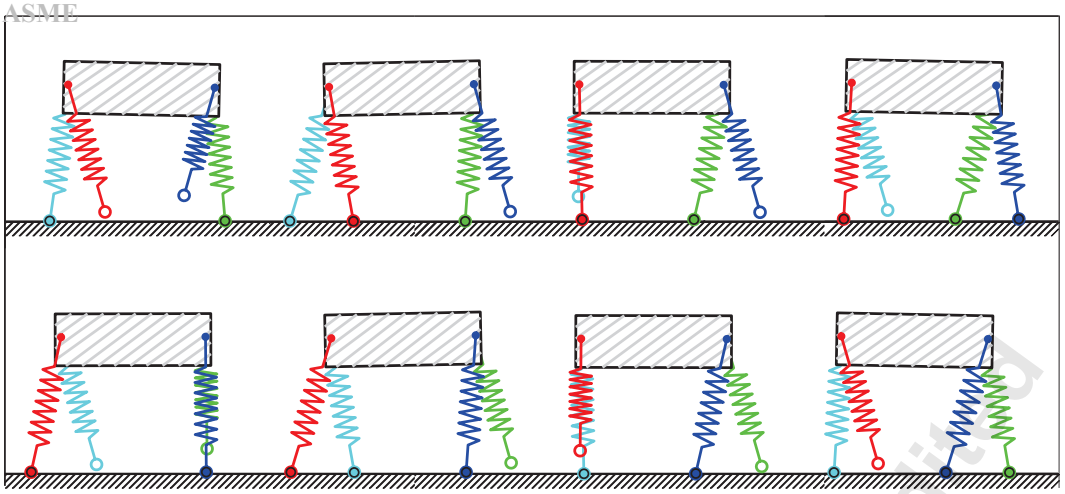

Fig. 4. 8 consecutive frames of a full stride of headless walking. The model is moving left to right. Uncompressed legs with open circels indicate legs that are *ready for touch-down* $(phase_i = 1)$, filled circles indicate legs that are in *stance* $(phase_i = 2)$, and retreacted legs are in *swing* $(phase_i = 3)$.

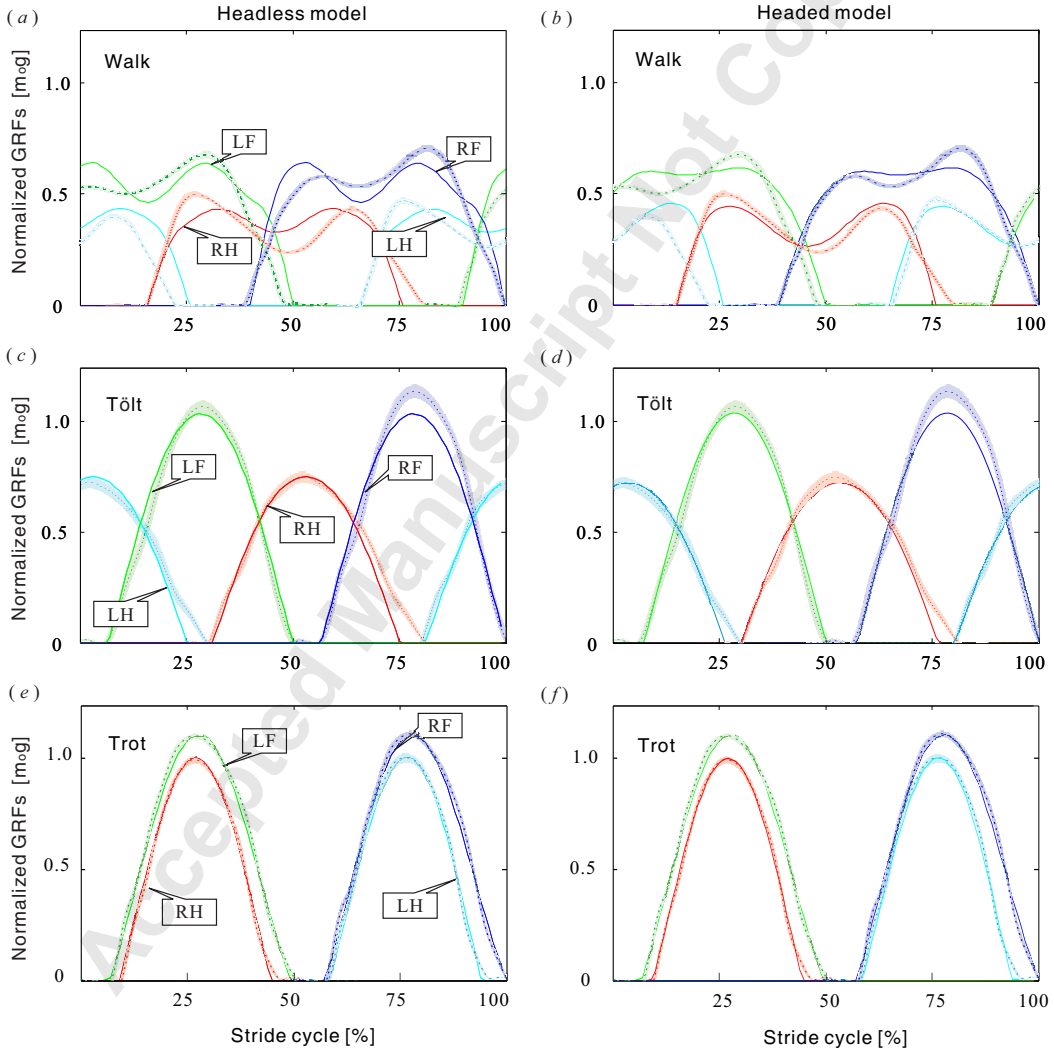

Fig. 5. Experimentally recorded vertical GRFs (dotted lines ± 1 std.) are compared to forces predicted by the headless model (solid lines, shown on the left) and to those predicted by the model with an articulated head and neck (solid lines, shown on the right). Shown are the results for walking (top), tölting (center), and trotting (bottom). Both models correctly predict the footfall pattern, timing, and the general shape of the force curves for all gaits. Quantitatively, a better fit is produced by the headed model, especially for the hind limbs at walk (see also Table 2). RH, RF, LH and LF stand for right hind, right fore, left hind, and left fore respectively.

tal data ($R^2 > 0.89$) (Table 2).

3.1.2 Tölt

The tölt is a symmetrical four-beat gait that is unique to Icelandic horses. It has the same footfall sequence as a walking gait. In contrast to walking, however, the legs spend less time on the ground and phases of double support alternate with phases of single support. Furthermore, each limb only undergoes a single compression cycle. The ground reaction forces have a single hump, similar to a bipedal running gait (Fig. 5c, d). Apart from the lift-off of the hind limbs, the model correctly predicts the footfall sequence, contact timing, and vertical GRFs. Individual GRFs are predicted with $R^2 > 0.96$.

Similar to walking, a clear but less pronounced pitching motion (-0.47° $+0.48^\circ$) of the main body can be observed. Even though the GRFs (and thus the spring compression) peak at almost twice the maximum value as for walking, the main body height y is fairly constant over the course of a stride. It only varies by $0.0058\,l_o$. Intra-stride horizontal velocity $\dot{x}$ is also nearly constant in this gait, and therefore velocity variability is the least among the gaits ($0.0317\,\sqrt{l_o g}$). In reality, the steady vertical and horizontal motion make this gait very comfortable for a rider. In simulation, the tölt had a velocity of $0.681\,\sqrt{l_o g}$, compared to a velocity of $0.975\,\sqrt{l_o g}$ recorded in the experiments.

3.1.3 Trot

The trot is a symmetrical two-beat gait, in which diagonal limb pairs move together. Phases of double support alternate with suspension phases. The vertical GRFs (Fig. 5e, f) show characteristic single humps that correspond to a single compression cycle of the leg spring. This result is similar to previous studies, which employed models that are more complex [24]. Of the three gaits, the trot is the gait that can be best approximated with our conceptual model. The overall GRFs are predicted with an R^2 value of more than 0.99. Similarly, the model predicts the contact sequence and the timing of touchdown and lift-off events with great accuracy. It is even able to account for the small differences in the contact timing and GRF-profiles between the two diagonal leg pairs. There is no visible pitching motion of the main body, yet a very pronounced vertical movement of about 0.04 leg lengths in y. Simulated trotting had a velocity of $0.559\,\sqrt{l_o g}$. Experimentally, this velocity was $0.893\,\sqrt{l_o g}$.

3.2 Sensitivity of Initial States and Parameters

For the sensitivity analysis of walking and trotting, each initial state and parameter value was varied by $\pm 1\,\%$. For tölting, which proved to be much more sensitive to both, states and parameters, we only varied their values by $\pm 0.05\,\%$. We excluded both the horizontal position x and the vertical position y from the analysis. The horizontal position x has no influence on the GRFs, and changing the vertical position y violates the lift-off condition at the terminal event $e^\star$. The results of the sensitivity study are shown in Figures 6.

In terms of sensitivity, there is quite some variability between different states and parameters. The forward velocity $\dot{x}$, for example, can be identified quite clearly, whereas the final cost value (or degree of fitting) is much less sensitive to the vertical velocity $\dot{y}$ and the pitch states φ and $\dot{\varphi}$. This holds for all three gaits. Related to the forward velocity, the angle of attack (for both, forelimbs and hind limbs) shows a larger sensitivity for all gaits and can thus be identified clearly.

Of the physical parameters, the quantity that can be identified best is the horizontal position of the center of mass (d_{COM}). Its value has a direct impact on the fore-aft distribution of the vertical GRFs and it is thus explicitly influencing the cost function. For walking and tölting, one can additionally identify the length and inertia of the main body, which are coupled to the vertical GRFs via the pitching dynamics of the main body. For trotting (which has hardly any pitching motion) these parameters cannot be identified accurately.

3.3 Headed Model

The same three gaits could be identified for the headed model. The initial continuous and discrete states for all gaits are listed in Tables 3 and 4, and the parameters in Tables 5 and 6. The resulting GRFs are shown in Figures 5. To assess the ability of this model to match the experimentally recorded vertical GRFs, the R^2 values are compared to those of the headless model in Table 2.

For the tölting and trotting gait, no clear improvement in the fitting to the experimental vertical GRFs was observed. Head and neck dynamics only play a minor role in these gaits, and the simplistic model without a head is good enough to explain the underlying motion. For walking, on the other hand, the head and neck motion does play an important role. Compared with the optimal solution of the headless model, the model with head improves the correlations of the GRFs of all four limbs significantly. On average, the fit improved by $4.35\,\%$. In particular, the asymmetry in the midstance relieve between forelimbs and hind limbs can only be explained with the additional head dynamics.

This observation also becomes clear when looking at the magnitude of the head motion. At the trot and tölt, the neck joint only rotates by 1.7 and 5.4 degrees, respectively. For walking, a rotation of over 15.1 degrees can be observed (Fig. 2) . With respect to parameters, the most notable change in the obtained solution is a decrease of d_{COM} (Table 5). Since the mass of the head would shift the overall location of the center of mass forward, the displacement of the main body COM (which is given by d_{COM}) is smaller as in the head-less case. This ensures that the impulse distribution and *overall* COM is still matching the experimental data.

4 Discussion and Conclusion

In this paper, we presented a simplistic passive dynamic model that is able to create realistic quadrupedal walking, tölting, and trotting motions. By choosing appropriate system parameters and initial states through an optimization

Table 3. Optimal initial continuous states for each gait. Please refer to Figure 1 for coordinate definitions

Gaits	$\dot{x}[\sqrt{l_o g}]$	$y[l_o]$	$\dot{y}[\sqrt{l_o g}]$	φ[rad]	$\dot{\varphi}[\sqrt{g/l_o}]$	θ[rad]	$\dot{\theta}[\sqrt{g/l_o}]$
Headless Walk	0.2601	0.9670	0.0100	-0.0208	0.0566	·	·
Headless Tölt	0.6818	0.9685	0.0148	0.0082	0.0349	·	·
Headless Trot	0.5701	0.9862	0.0417	-0.0126	0.0065	·	·
Headed Walk	0.3236	0.9604	-0.0045	-0.0351	0.0731	0.4186	-0.2921
Headed Tölt	0.8737	0.9656	0.0182	0.0076	0.0334	0.7927	-0.1942
Headed Trot	0.6490	0.9866	0.0393	-0.0103	0.0064	0.3388	-0.0329

Table 4. Initial discrete states for each gait. Listed are for each leg the phases ('ready for touch down' (1),'stance' (2), or 'swing' (3)), and the horizontal foot positions in absolute coordinates. RH, RF, LH and LF stand for right hind, right fore, left hind, and left fore respectively. For legs that are in the air, the foot position records where the foot was before lift-off. Note that all gaits start with the right forelimb in swing

Gaits	$phase_{LH}[\cdot]$	$phase_{RH}[\cdot]$	$phase_{LF}[\cdot]$	$phase_{RF}[\cdot]$	$pos_{LH}[l_o]$	$pos_{RH}[l_o]$	$pos_{LF}[l_o]$	$pos_{RF}[l_o]$
Headless Walk	2	1	2	3	-0.6708	-1.1352	0.6121	0.1477
Headless Tölt	2	1	1	3	-0.5441	-1.0850	-0.3414	0.1995
Headless Trot	3	1	1	3	-0.7688	-1.2293	-0.2419	0.2304
Headed Walk	2	1	2	3	-0.5519	-1.0877	0.6611	0.1253
Headed Tölt	2	1	1	3	-0.5364	-1.1057	-0.2537	0.3156
Headed Trot	3	1	1	3	-0.7914	-1.2533	-0.0792	0.3960

Table 5. Optimal main body parameter choices for each gait. Please note that d_{COM} only reflects the main-body COM, not the overall value. It is smaller for the headed model, since there is additional mass in the head-neck segment

Gaits	$m_1[m_o]$	$l_1[l_o]$	$j_1[m_o l_o^2]$	$k_H[m_o g/l_o]$	$k_F[m_o g/l_o]$	α_H[rad]	α_F[rad]	$d_{COM}[\cdot]$	$t_{swing}[\sqrt{l_o/g}]$
Headless Walk	1.00	1.06	0.28	18.31	24.69	0.28	0.28	0.59	0.58
Headless Tölt	1.00	1.01	0.42	20.60	24.88	0.24	0.24	0.57	0.41
Headless Trot	1.00	0.96	0.80	21.46	19.83	0.16	0.20	0.56	0.50
Headed Walk	0.87	0.95	0.25	14.26	15.50	0.33	0.33	0.52	0.55
Headed Tölt	0.89	1.13	0.67	18.65	23.33	0.27	0.25	0.51	0.42
Headed Trot	0.86	1.15	1.15	25.18	21.87	0.16	0.20	0.49	0.43

Journal of Computational and Nonlinear Dynamics. Received February 10, 2015;
Accepted manuscript posted May 14, 2015. doi:10.1115/1.4030622

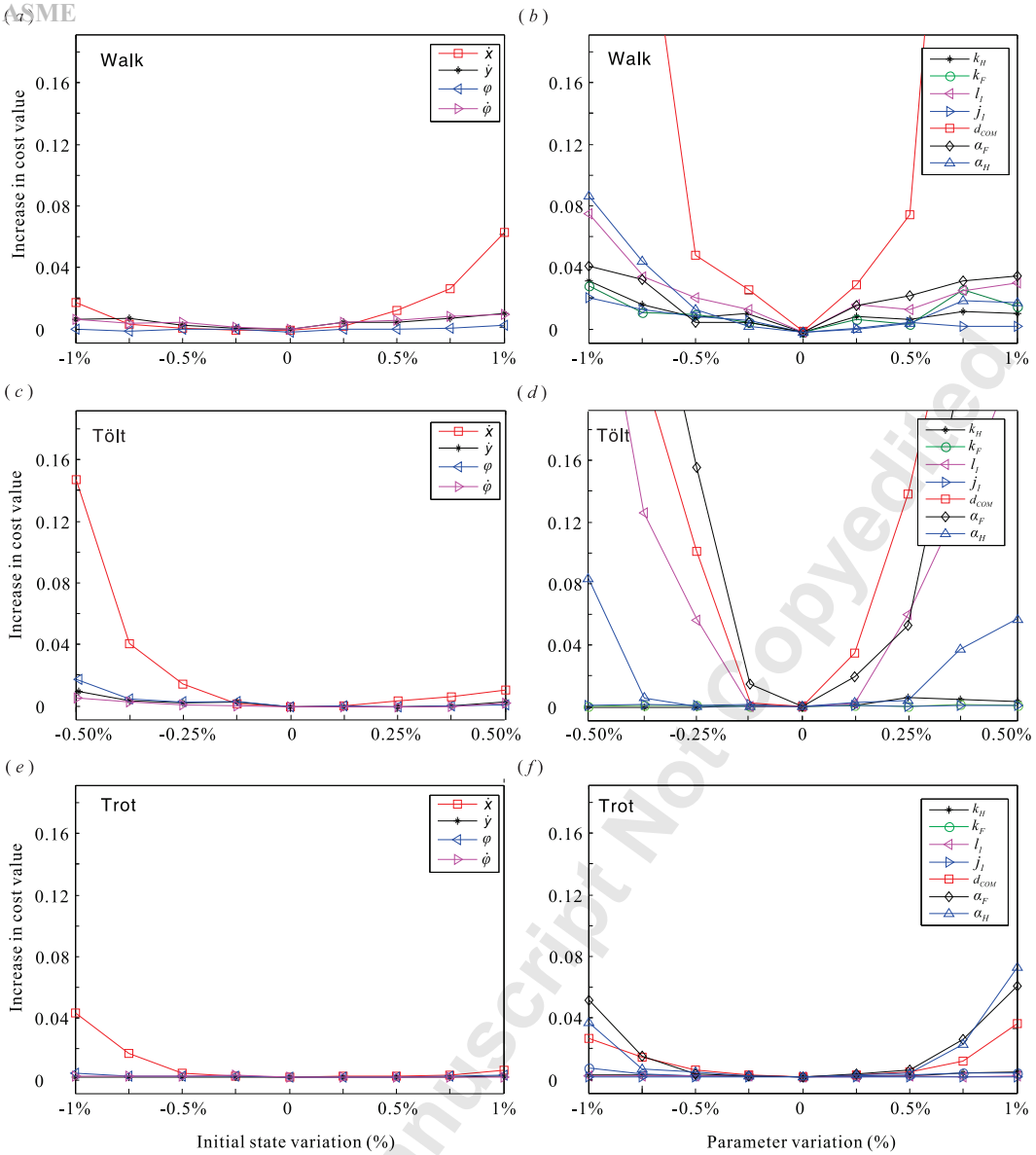

Fig. 6. Shown is the increase in cost (quantifying the difference between model-predicted and experimentally measured vertical GRFs) as a function to variations in states (shown on the left) and parameter choices (shown on the right). Results are shown for walking (top), tölting (center), and trotting (bottom). This analysis highlights which states and parameters can be predicted well by matching of the vertical GRFs (indicated by a high sensitivity) and which cannot be predicted well (indicated by a low sensitivity).

process, the model is able to closely match the GRFs of walk and trot in Warmblood horses and of tölt in Icelandic horses. We investigated the sensitivity of the obtained solutions with respect to all states and parameters, and evaluated the improvement in fitting GRFs when including an additional head and neck segment.

4.1 Generating Multiple Gaits with a Single Model

Our proposed model generates this variety of different gaits primarily by altering the initial continuous and discrete states of the system. The resulting motions, footfall patterns, and GRFs emerge from these initial conditions through a numerical integration of the dynamics. Our finding suggests that quadrupedal gaits are merely different dynamic modes of the same structural system and that we can interpret different gaits as different nonlinear elastic oscillations that propel an animal forward. These different oscillation modes create a large variety of locomotion types and allow for varying properties (such as different locomotion velocities) that can be exploited by the animal.

The main determinant for a particular gait (or footfall pattern) are the initial phase choices (Table 4). For walk, the model starts with both left limbs in stance; for tölt, only the left hind limb is in stance; and for trot all legs are in the air. The *ready for touch down* phase indicates additionally which feet are able to strike the ground next. For walk this is the right hind limb, and for tölt and trot the right hind limb and left forelimb. The exact timing of these footfalls, however, is determined by the continuous states. Remember that all gaits

Table 6. Optimal choices for the head parameters for each gait

Gaits	$m_2[\mathrm{m_o}]$	$l_2[\mathrm{l_o}]$	$j_2[\mathrm{m_o l_o^2}]$	$k_{head}[\mathrm{m_o g l_o/rad}]$	$\theta_{rest}[\mathrm{rad}]$
Headed Walk	0.13	0.69	0.07	1.30	0.38
Headed Tölt	0.11	0.51	0.22	3.25	0.85
Headed Trot	0.14	0.74	0.11	2.37	0.39

Table 7. Comparison of simulated and experimental stride time

Gaits	Experiments [s]	Simulation [s]
Headless Walk	1.129	1.402
Headless Tölt	0.523	0.548
Headless Trot	0.825	0.649
Headed Walk	1.129	1.281
Headed Tölt	0.523	0.536
Headed Trot	0.825	0.569

are assumed to start at lift-off of the right forelimb.

In addition to the starting conditions, the motion is influenced by the system parameters. Some of these parameters, such as the angles of attack α or the rest angle of the neck θ_{rest} would represent a concious choice of the animal and are expected to change from gait to gait. Other parameters are fixed physical properties that would not vary in a real horse. Yet, in our study, we did allow all values to change, in order to account for the fact that the experimental data was recorded from different horses. Despite being unconstrained, the main parameters (such as the main body length l_1, leg stiffness k, or COM position d_{com}) had very similar values for the three gaits (Tables 5 & 6).

A detailed analysis of the stability of the obtained motions was not the focus of our work. However, a quick check of the Floquet-multipliers revealed that all reported motions are unstable in a linear approximation. Values varied from 3.2 for headless walking to 247 for the headless tölt. That means, while the gaits that we identified are periodic, continuous locomotion can only be maintained in the complete absence of disturbances. Even a tiny deviation from the periodic orbit will eventually lead to a fall. With this in mind, the presented motions can only be considered as nominal. For continuous locomotion, they must be stabilized through appropriate active feedback control.

The main methodological improvement that enabled us to find multiple gaits within a single model was the introduction of a 'swing phase' in the simulation. In this phase, the feet are unable to engage in ground contact. This facilitated the intrinsic coordination of complex motion patterns and allowed us to include all four limbs in the simulation at the same time. This made it unnecessary to make additional assumptions (such as synergies and symmetries [10]), or to artificially reduce the complexity of the model (e.g., to a single spring mass system [9] or to the lateral half of a quadruped [25]). In contrast to these examples in which the models could only be used for the parametric analysis of *specific* gaits (such as a trotting or bounding), our proposed model can produce a much larger number of gaits; including the complex motions of four-beat walking and tölting. At the same time, the complexity of the simulation and the number of necessary parameters remains at an absolute minimum. Despite this simplicity, the model does not only produce qualitatively different motion patterns, but can quantitatively match recorded vertical GRFs with high accuracy. Particularly the GRFs of trotting and tölting can be predicted almost perfectly. Larger residuals were only obtained when identifying walking, but could be alleviated by adding a head-neck segment to the model.

4.2 Stride Time

The cost function in eq. 5 uses a normalized time to speed up the optimization process and to get better convergence. The goal of this research was to identify the footfall sequence and shapes of vertical GRFs for different gaits of horses in nature by using simple models. Stride time was thus not our primary concern. However, for comparison, the absolute stride time (in seconds) is listed in Table 7 for both the optimized simulated results and the experimental data. Larger discrepancies can be observed in the trotting gait of both headless and headed models as well as in headless walk.

4.3 Model Limitations and Comparison to Biology

Naturally, a simplistic model has to make some approximations and can never fully explain all observed dynamics. In the following, we compare our results to the locomotion of horses in nature and discuss the limitations that are inevitable when using such strongly simplified models.

The passive nature of our models prevents an active contribution to the motion; for example, during an active push-off. The lift-off of all limbs shows a pronounced break-over phase in the experimentally recorded GRFs. In nature, this prolongation of the stance phase is caused by the hoof tilting actively shortly before lift-off. Such an effect cannot be replicated in our models, where the point-feet predict abruptly vanishing vertical GRFs. The break-over influence is visible in all gaits but most prominent at tölt in the hind limbs (Fig. 5c, d). This may be caused by the comparatively larger range of the limb angle in Icelandic horses compared to Warmblood horses; especially while tölting [26, 27].

Since our models are planar, they are unable to replicate motions that happen outside the sagittal plane. As the

experimental GRFs are mostly symmetric with respect to left and right, this did not cause any major problems. The only exemption are the forelimb forces of the tölt, in which the experimentally measured peak force of the right side was significantly higher than the peak force of the left side (Fig. 5c, d). This is potentially caused by a lateral torso motion. Such an asymmetric loading cannot be produced with the planar symmetrical model. This does not mean that we can only generate symmetrical gaits. For example, there is an asymmetry regarding the leg phasing of the diagonal legs at trot in the experimental data. For the left diagonal (LF, RH) the impact of the RH limb is slightly delayed with reference to the LF impact, while the legs of the right diagonal (RF, LH) impacted nearly synchronously. This behavior can be replicated in simulation and explained by a small difference in the main body pitch between the two diagonal stances (Fig. 5e, f). Even a small amount of such pitch influences the relative timing of fore and hind footfall. Furthermore, we have shown in related work that our planar model can produce the footfall patterns associated with asymmetric gaits such as bounding or galloping [19].

In terms of methodology, we based our gait identification on the replication of vertical GRFs. Our cost function was the difference between measured and model-predicted GRFs. This is a reasonable choice, since the GRFs contain substantial gait information; including contact sequences, footfall timing, and center of mass dynamics. Yet, when comparing the model-predicted optimal parameter choices and resulting motion characteristics to values reported from biology, one should keep in mind that not all parameters can be identified with the same accuracy by our optimization method. We evaluated this effect in a sensitivity study that investigated how well each state and parameter could be identified. The GRFs of the trot, for example, are clearly dependent on the center of mass position d_{COM}, but they are not very sensitive to the main body length l_1 and inertia j_1 (Fig. 6f). This means that d_{COM} can be accurately identified, while our method does not allow clear conclusions about the values of l_1 and j_1. This is not surprising. At trot, the main body is mostly leveled and not undergoing a large amount of pitch. Since length and inertia are parameter values that can only manifest themselves in the GRFs if the main body is pitching, they are consequently not reflected in the analysis of a trot. At walk and tölt, on the other hand, a pronounced pitching motion exists, and the analysis is very sensitive to l_1 and j_1 (Fig. 6b, d).

An interesting result of the sensitivity study was the low predictability of the leg stiffness values. Independent of the chosen gait, it was shown that the leg stiffness could not be predicted through the analysis of the GRFs. This is surprising, since the leg stiffness appears to be one of the most fundamental model properties and should have a direct influence on the GRFs. However, a simultaneous adaptation of the motion (most notably through the vertical velocity $\dot{y}$ and the pitch states φ and $\dot{\varphi}$) can compensate for this effect, such that the combination of leg stiffness and vertical motion cannot be resolved from the GRFs alone. Furthermore, this effect might also be amplified by the normalization of stride duration in eq. (5). Having no absolute time in the model potentially degrades the correct identification of frequencies.

In terms of identifying motions and parameters, some limitations might arise from the fact that we were experimentally limited to *vertical* contact forces. Consequently, we had only limited knowledge about the fore-aft motion. Characteristics that relate to this motion could not be identified very well. For example, the model-predicted forward velocities differed substantially from the experimentally recorded values. At walk, the model-predicted speed was about half of the experimentally measured. This shortcoming is likely a consequence of the missing horizontal contact information.

Furthermore, redundancies in the model can make it difficult to identify values reliably. This can be seen, for example, with respect to the head-neck parameters. In order to match experimental GRFs, the optimizer had to synchronize the head-neck motion with the pitching of the main body. The two motions must be exactly out of phase at tölt and especially at walk (Fig. 2). That is, the natural frequency of the neck oscillation must be matched to the overall stride frequency. Through this link of morphology, motion, and contact forces, the optimizer can establish estimates of parameter values through matching of the GRFs. Yet, since four morphologic parameters (head length l_2, head and neck stiffness k_{head}, head mass m_2, and inertia j_2) all influence the natural frequency of the head motion, it becomes difficult to determine all these parameters at the same time. This is reflected in the large variability that some of these parameters have for the three different gaits (Table 6).

Even with these limitations, parameters were often close to values reported in biology (using [28] as our main reference). This holds, for example, for the overall COM position at walk of 59 % of the main body (in the headless case this is identical to d_{COM}, Table 5), compared to a value of 58.2 % in Warmblooded horses [29]. For trotting the model predicts 56 % compared to 57.0 %. Similarly, the model predicts a main body length l_1 between $0.95\,l_o$ and $1.15\,l_o$ which compares to values of about $0.8\,l_o$ in horses. This list includes even more detailed parameters, such as the relative amount of the head and neck mass. The predicted value of 11 %-14 % (Tables 5 & 6) only slightly overestimates values from the existing literature, where head-neck mass was determined as about 8 % of body weight [30]. While the optimization outcomes are not exact predictions, they show that the model parameters are in the right ballpark.

4.4 Outlook and Future Work

A natural continuation of our work is to extend the presented study to additional gaits, including asymmetrical gaits such as bounding and gallopping. As mentioned earlier, the footfall patterns associated with these gaits can be produced by our models, yet a quantitative comparison to experimentally recorded data is still missing. In the same framework, one could also investigate the effect of varying gait parameters such as locomotion speed or carried loads.

In this study, we were able to find a full range of possible motions for each footfall pattern, and only by matching

the motion to experimental data, we were able to produce unique solutions. On a theoretical level, it would be valuable to investigate the boundaries of these different solution classes, thereby answering questions such as: Is there a maximal speed for a walking footfall sequence? Do gaits 'blend' into each other continuously, or are there distinct transitions? While passive models cannot predict gait changes driven by energetics (as shown for example by [31]), it might be possible to explain more fundamental limits in the use of different gaits. This knowledge does not only improve our understanding of locomotion in nature, but might be used in the design of legged robots, which could benefit from multiple gaits similarly as animals and humans.

Acknowledgement

This material is based upon work supported by the National Science Foundation under Grant No. 1453346. Funding for this project was provided by NIH (GRANT: 1-R01-EB019834-2014 "Wearable eMbots to Induce Recovery of Function").

References

[1] Cavagna, G. A., and Kaneko, M., 1977. "Mechanical work and efficiency in level walking and running". *The Journal of Physiology,* **268**(2), pp. 467–481.

[2] McGeer, T., 1990. "Passive dynamic walking". *The International Journal of Robotics Research,* **9**(2), pp. 62–82.

[3] Seyfarth, A., Geyer, H., Günther, M., and Blickhan, R., 2002. "A movement criterion for running". *Journal of biomechanics,* **35**(5), pp. 649–655.

[4] Cavagna, G. A., Heglund, N. C., and Taylor, C. R., 1977. "Mechanical work in terrestrial locomotion: two basic mechanisms for minimizing energy expenditure". *American Journal of Physiology-Regulatory, Integrative and Comparative Physiology,* **233**(5), pp. R243–R261.

[5] Mochon, S., and McMahon, T. A., 1980. "Ballistic walking: An improved model". *Mathematical Biosciences,* **52**(3), pp. 241–260.

[6] Garcia, M., Chatterjee, A., Ruina, A., and Coleman, M., 1998. "The simplest walking model: stability, complexity, and scaling". *Journal of biomechanical engineering,* **120**(2), pp. 281–288.

[7] Kuo, A. D., 1999. "Stabilization of lateral motion in passive dynamic walking". *The International journal of robotics research,* **18**(9), pp. 917–930.

[8] Geyer, H., Seyfarth, A., and Blickhan, R., 2006. "Compliant leg behaviour explains basic dynamics of walking and running". *Proceedings of the Royal Society B,* **273**(1603), pp. 2861–2867.

[9] Farley, C. T., Glasheen, J., and McMahon, T. A., 1993. "Running springs - speed and animal size". *Journal of Experimental Biology,* **185**, pp. 71–86.

[10] Full, R. J., and Koditschek, D. E., 1999. "Templates and anchors: neuromechanical hypotheses of legged locomotion on land". *Journal of Experimental Biology,* **202**(23), pp. 3325–3332.

[11] Lee, C. R., and Farley, C. T., 1998. "Determinants of the center of mass trajectory in human walking and running.". *Journal of Experimental Biology,* **201**(21), pp. 2935–2944.

[12] Pandy, M. G., 2003. "Simple and complex models for studying muscle function in walking". *Philosophical Transactions of the Royal Society of London. Series B: Biological Sciences,* **358**(1437), pp. 1501–1509.

[13] Smith, A. C., and Berkemeier, M. D., 1997. "Passive dynamic quadrupedal walking". In International Conference on Robotics and Automation, ICRA, Vol. 1, pp. 34–39.

[14] Remy, C. D., Buffinton, K. W., and Siegwart, R. Y., 2010. "Stability analysis of passive dynamic walking of quadrupeds". *The International Journal of Robotics Research,* **29**(9), pp. 1173–85.

[15] Remy, C. D., Hutter, M., and Siegwart, R., 2010. "Passive dynamic walking with quadrupeds - extensions towards 3d". In International Conference on Robotics and Automation, ICRA, pp. 5231 – 5236.

[16] McGuigan, M. P., and Wilson, A. M., 2003. "The effect of gait and digital flexor muscle activation on limb compliance in the forelimb of the horse equus caballus". *Journal of Experimental Biology,* **206**(8), pp. 1325–1336.

[17] Clayton, H. M., Schamhardt, H. C., Willemen, M. A., Lanovaz, J. L., and Colborne, G. R., 2000. "Kinematics and ground reaction forces in horses with superficial digital flexor tendinitis". *American journal of veterinary research,* **61**(2), pp. 191–196.

[18] Remy, C. D., Buffinton, K., and Siegwart, R., 2011. "A matlab framework for efficient gait creation". In Intelligent Robots and Systems (IROS), 2011 IEEE/RSJ International Conference on, IEEE, pp. 190–196.

[19] Gan, Z., and Remy, C. D., 2014. "A passive dynamic quadruped that moves in a large variety of gaits". In International Conference on Intelligent Robots and Systems, IROS, p. (under review).

[20] Hof, A. L., 1996. "Scaling gait data to body size". *Gait & Posture,* **4**(3), pp. 222–223.

[21] Weishaupt, M. A., Hogg, H. P., Wiestner, T., Denoth, J., Stüssi, E., and Auer, J. A., 2002. "Instrumented treadmill for measuring vertical ground reaction forces in horses". *American journal of veterinary research,* **63**(4), pp. 520–527.

[22] Griffin, T. M., Kram, R., Wickler, S. J., and Hoyt, D. F., 2004. "Biomechanical and energetic determinants of the walk–trot transition in horses". *Journal of Experimental Biology,* **207**(24), pp. 4215–4223.

[23] Geyer, H., Seyfarth, A., and Blickhan, R., 2006. "Compliant leg behaviour explains basic dynamics of walking and running". *Proceedings of the Royal Society B: Biological Sciences,* **273**(1603), pp. 2861–2867.

[24] Herr, H. M., and McMahon, T. A., 2000. "A trotting horse model". *The International Journal of Robotics Research,* **19**(6), pp. 566–581.

[25] Chatzakos, P., and Papadopoulos, E., 2007. "Parametric analysis and design guidelines for a quadruped bounding robot". In Control & Automation, 2007. MED'07. Mediterranean Conference on, IEEE, pp. 1–6.

[26] Weishaupt, M., Waldern, N., Kubli, V., and Wiestner, T., 2014. "Effects of shoeing on breakover forces in icelandic horses at walk, tölt and trot". *Equine Veterinary Journal,* **46**(S46), pp. 51–51.

[27] Bogisch, S., Geser-Von Peinen, K., Wiestner, T., Roepstorff, L., and Weishaupt, M., 2014. "Influence of velocity on horse and rider movement and resulting saddle forces at walk and trot". *Comparative Exercise Physiology,* **10**(1), pp. 23–32.

[28] Vorstenbosch, M., Buchner, H., Savelberg, H., Schamhardt, H., and Barneveld, A., 1997. "Modeling study of compensatory head movements in lame horses.". *American journal of veterinary research,* **58**(7), pp. 713–718.

[29] Waldern, N., Wiestner, T., Peinen, K. v., Álvarez, C., Roepstorff, L., Johnston, C., Meyer, H., and Weishaupt, M., 2009. "Influence of different head-neck positions on vertical ground reaction forces, linear and time parameters in the unridden horse walking and trotting on a treadmill". *Equine veterinary journal,* **41**(3), pp. 268–273.

[30] Buchner, H., Savelberg, H., Schamhardt, H., and Barneveld, A., 1997. "Inertial properties of dutch warmblood horses". *Journal of biomechanics,* **30**(6), pp. 653–658.

[31] Hoyt, D. F., and Taylor, C. R., 1981. "Gait and the energetics of locomotion in horses". *Nature,* **292**(5820), pp. 239–240.

List of Figures

List of Tables

Appendix A: EOM of the Headed Model

The equations of motion of the headed model were derived using the Euler-Lagrange equations. The mass matrix is given as:

$$M = \begin{bmatrix} m_1+m_2 & 0 & C_1 & -m_2 l_2 \sin(\varphi+\theta) \\ 0 & m_1+m_2 & C_2 & m_2 l_2 \cos(\varphi+\theta) \\ C_1 & C_2 & C_3 & C_4 \\ -m_2 l_2 \sin(\varphi+\theta) & m_2 l_2 \cos(\varphi+\theta) & C_4 & m_2 l_2^2 + j_2 \end{bmatrix}, \tag{17}$$

with

$$\begin{aligned} C_1 &= -m_2 d_F \sin(\varphi) - m_2 l_2 \sin(\varphi+\theta), \\ C_2 &= m_2 d_F \cos(\varphi) + m_2 l_2 \cos(\varphi+\theta), \\ C_3 &= m_2 d_F^2 + m_2 l_2^2 + 2 m_2 d_F l_2 \cos(\theta) + j_1 + j_2, \\ C_4 &= m_2 l_2^2 + m_2 d_F l_2 \cos(\theta). \end{aligned}$$

The Coriolis, centrifugal, and gravitational terms are given as:

$$h = -\begin{bmatrix} (\dot\varphi+\dot\theta)^2 l_2 m_2 \cos(\varphi+\theta) + \dot\varphi^2 d_F m_2 \cos(\varphi) \\ (\dot\varphi+\dot\theta)^2 l_2 m_2 \sin(\varphi+\theta) + \dot\varphi^2 d_F m_2 \sin(\varphi) - (m_1+m_2) g \\ m_2 \dot\theta^2 d_F l_2 \sin(\theta) + 2 m_2 \dot\varphi \dot\theta d_F l_2 \sin(\theta) - m_2 g d_F \cos(\theta) - m_2 g l_2 \cos(\varphi \\ -m_2 \dot\varphi^2 l_2 d_F \sin(\theta) - m_2 g l_2 \cos(\varphi+\theta) \end{bmatrix} \tag{18}$$

The generalized forces additionally include the torque M_{head} that is produced by the head and neck spring-damper. The leg forces and the neck torque are projected into the generalized coordinates according to:

$$\tau = \sum_i J_i^T F_i + J_{head}^T M_{head} \tag{19}$$

$$\begin{aligned} \mathbf{J}_i &= [-\sin(\gamma_i),\ \cos(\gamma_i),\ d_i \cdot cos(\varphi-\gamma_i),\ 0] \\ \mathbf{J}_{head} &= [0\ 0\ 1\ 1] \end{aligned} \tag{20}$$